

SYNTHESIS OF POLY-SILICON THIN FILMS ON GLASS SUBSTRATE USING LASER INITIATED METAL INDUCED CRYSTALLAZATION OF AMOURPHOUS SILICON FOR SPACE POWER APLLICATION

Husam H. Abu-Safe, Hameed A. Naseem, and William D. Brown, Department of Electrical Engineering, Arkansas Photovoltaic Research Center, University of Arkansas, Fayetteville, AR*

Abstract

Poly-silicon thin films on glass substrates are synthesized using laser initiated metal induced crystallization of hydrogenated amorphous silicon films. These films can be used to fabricate solar cells on low cost glass and flexible substrates. The process starts by depositing 200 nm amorphous silicon films on the glass substrates. Following this, 200 nm of sputtered aluminum films were deposited on top of the silicon layers. The samples are irradiated with an argon ion cw laser beam for annealing. Laser power densities ranging from 4 to 9 W/cm² were used in the annealing process. Each area on the sample is irradiated for a different exposure time. Optical microscopy was used to examine any cracks in the films and loss of adhesion to the substrates. X-Ray diffraction patterns from the initial results indicated the crystallization in the films. Scanning electron microscopy shows dendritic growth. The composition analysis of the crystallized films was conducted using Energy Dispersive x-ray Spectroscopy. The results of poly-silicon films synthesis on space qualified flexible substrates such as Kapton[®] are also presented.

*Email: habusaf@engr.uark.edu

Introduction

The formation of polycrystalline silicon (poly-Si) by annealing its amorphous precursor has been receiving a great deal of attention due to the immense potential it has in large area microelectronic applications. Poly-Si thin films can be used to fabricate thin film solar cells, thin film transistors for active matrix liquid crystal displays (AMLCDs), image sensors and also in 3D microelectronics. While there are many techniques to make poly-Si thin films by direct deposition or by crystallizing amorphous silicon (a-Si) films deposited on foreign substrates, metal induced crystallization (MIC) has been viewed as the best technique so far to fabricate continuous thin polycrystalline films on cheap substrates like glass and plastic. This is because of the low temperatures, simple processing steps, and very small processing times involved in this particular method. It is well known that amorphous silicon, when in contact with certain metals and subjected to thermal annealing crystallizes at very low temperatures. Various metals such as Al (1), Ag (2), Pd (3), Ni (4), and Au (5), have been used to crystallize a-Si films using this method. In the case of Al, temperatures as low as 150°C have been reported (6). The excitation sources for the interaction between metal-Si interfaces in most of the studies were thermal annealing, microwave annealing, ion beam sources and electric field. Laser crystallization (LC) technique has been widely investigated in the creation of poly-Si thin films for more than a decade. Using ultra-short pulsed laser irradiation to crystallize a-Si thin has shown that non-thermal effects are responsible for the phase transition in the films (7). However, long pulses and cw irradiation result in thermal activation of the crystallization process (8). Until now, all studies based on MIC used thermal annealing as an excitation source. In our study, we use laser powers to initiate the a-Si crystallization process.

Experiment

Two sets of samples were prepared in this study. In the first set, 0.15 mm thick clean cover glass (Soda lime glass) substrates were used to deposit 200 nm hydrogenated amorphous silicon (a-Si:H). Plasma enhanced chemical vapor deposition (PECVD) was used for this deposition. The deposition took place under the following conditions: prior to deposition, the pressure inside the deposition chamber was brought down to 10^{-8} Torr and the substrate temperature was set to 250°C. SiH_4 gas was then introduced to the chamber at 20 sccm flow rate. When the pressure in the chamber reached 0.5 Torr, 4 W of RF power was applied to create the plasma. Under these conditions, the deposition rate was estimated to be 13 nm/min. When the deposition was complete the samples were transferred to an Al sputtering chamber without breaking the vacuum. There, argon gas with a flow rate of 20 sccm was used to sputter deposit 100 nm of Al layer on top of the a-Si:H at 40°C. For the second set of samples, flexible Kapton sheets with 7 μm thickness were used as substrates to deposit a-Si:H films under the same deposition conditions. Sputtered Al (100 nm) was deposited on the a-Si films in this set also. A 3.0 W cw argon-ion laser ($\lambda=514.5\text{nm}$) with 2 mm beam diameter was used to irradiate the samples from the substrate side (see Fig. 1). The laser beam was expanded using a 10 cm converging lens. The laser power density was varied simply by changing the sample position with respect to the beam waist ω_0 . The beam waist is taken to be the distant from the center of the Gaussian beam to the point where the intensity of the beam reduces to I_0/e^2 . The samples were irradiated for various exposure times at 4, 6 and 9 W/cm^2 . The laser beam was used to create one spot with a constant power density and exposure time. However, the Kapton samples were scanned by the laser beam without expanding at speed of 2.4 mm/sec. The power density in this case was varied by changing the laser output power. Optical images of the samples were used to check for crack and loss of adhesion to the substrate. X-ray diffraction (XRD) technique was used to investigate crystallization in the samples. Scanning electron microscope (SEM) images used to explore the morphology of the laser-irradiated regions. These images were taken before and after removing the Al films in the samples. The Al film was removed using standard Al etching solution (85% phosphoric acid, 5% nitric acid, 5% acetic acid, and 5% DI water at 40°C). Energy Dispersive x-ray Spectroscopy (EDX) was used in this study to identify the film composition.

Results and discussion

Optical Microscopy

Fig. 2 shows optical microscope images of the samples irradiated by the laser beam at different power densities before and after Al etching. The images were taken at the spot center. At $4\text{W}/\text{cm}^2$, black spots are observed on the Al surface. This indicates that some interaction was occurring at this power density. However,

when Al was etched off, the Si films were still in the amorphous state. This was confirmed from the optical images and the XRD measurements.

At $6\text{W}/\text{cm}^2$, more of these black spots appeared on top of the Al surface. When the Al was etched, the morphology of the silicon surface resembled that of the Al. This indicated strong interaction between the two film layers. No cracks or peeling was observed in the silicon film. The silicon surface appeared to have large number of grains connected together. These grains were bigger when the samples were irradiated with $9\text{W}/\text{cm}^2$ as shown in Fig 2 (c).

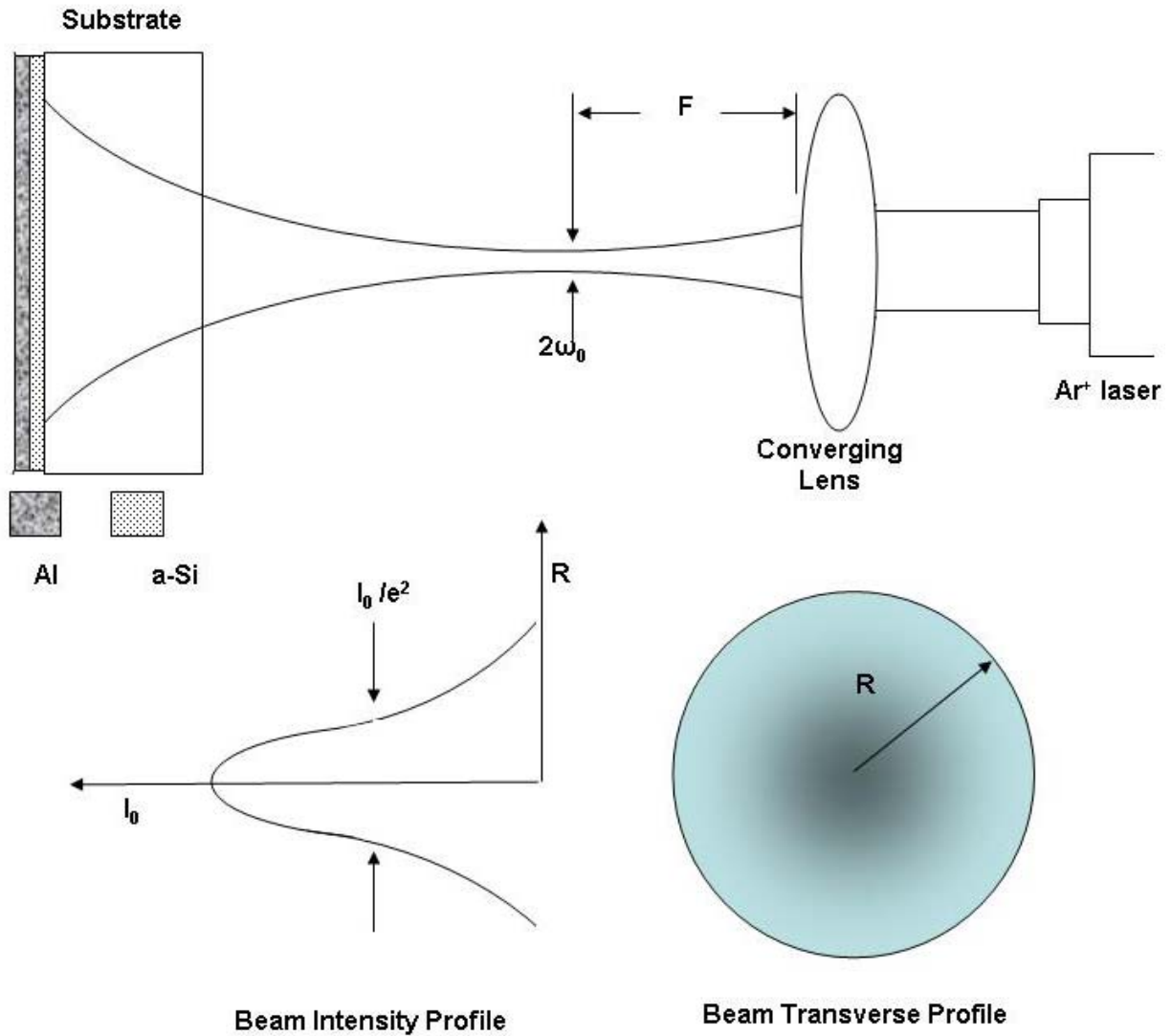


Fig. 1: Schematics of the experimental set up. The 2 mm radius Ar⁺ laser beam was expanded using a converging lens. The beam radius (**R**) is taken to be the distant from the center of the Gaussian beam to the point where the intensity of the beam reduces to I_0/e^2 . The beam was used to create one spot on the glass samples at different power densities and exposure times.

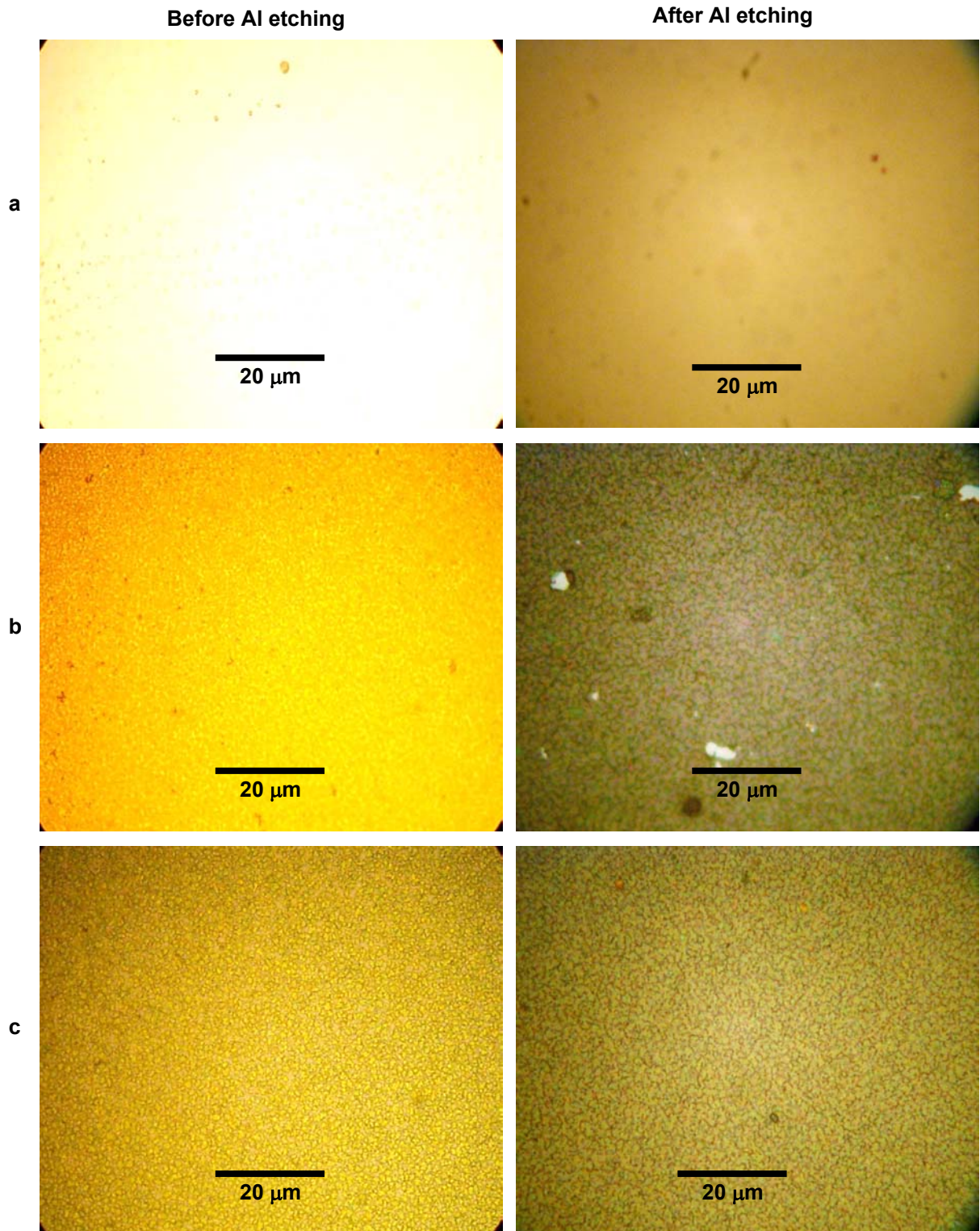


Fig. 2: Optical images of the irradiated samples for 3 minutes at different power densities. a) $4\text{W}/\text{cm}^2$ b) $6\text{W}/\text{cm}^2$ c) $9\text{W}/\text{cm}^2$.

Fig. 3 shows the optical images of silicon films deposited on the Kapton substrates. These images are taken after Al is etched off. The power density was changed by changing the laser output power. The laser beam spot size was taken to be 1 mm. It can be seen from the figure that as the laser power density increase, more of the silicon grains appear. At 9 W/cm² the silicon film looks continuous without any cracks or peeling.

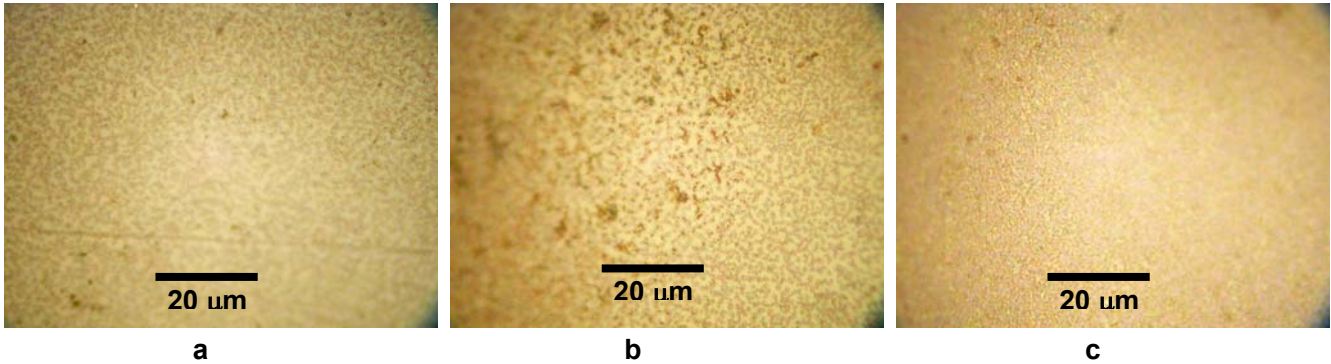


Fig. 3: Optical images of silicon film on the Kapton substrates. The samples were scanned with a laser beam at: a) 4W/cm² b) 6W/cm² c) 9W/cm². The scanning speed was 2.4 mm/sec.

X-ray Diffraction

XRD plots of the samples on glass substrates irradiated with 6 and 9 W/cm² power densities with a constant exposure time are shown in Fig. 4. It is clearly evident from the figures that the resulting films are polycrystalline in nature. The broad hump for a-Si is not seen and the Si (111) peak at 28.5° indicates the crystallization in these films. The XRD plots of the samples irradiated at 4 W/cm² did not show any silicon peak, which means that no crystallization was possible at this power density. The amount of crystallization in the irradiated sample was measured by monitoring the Si (111) peak. No significant difference in the Al (111) peak at around 38.5° was observed with changes in laser power densities or exposure time. I

It is clear from Fig. 4(a) that crystallization was initiated for the initial power density of 6 W/cm² after 1 minute of exposure time. The Si peak intensity started to grow with this exposure time. We measured the silicon peak area at each power density as a function of the sample exposure time. These measurements are shown in Fig. 5. The peak area increases with increasing power density and irradiation time. However, after 3 minutes this increase becomes smaller indicating saturation in the crystallized volume of these samples. At 9 W/cm² the rate of increase in the silicon peak is much smaller than that obtained for the 6 W/cm² irradiated samples up to 3 minutes. This means that the crystallization at this power density reached its saturation within the first minute of irradiation time whereas, for the 6 W/cm² exposure samples it did not occur until 3 minutes. It must be noted here; however, that the amount of crystallization at 9 W/cm² was anywhere 2 to 3 times that for 6W/cm².

The crystallization rate in the films can be computed by calculating the slopes of the curves in Fig. 5. Assuming that there is no growth rate when there is no laser beam, we got slopes of 4.5 and 6.8 for the 6 and 9 W/cm² curves, respectively. In general, when the crystallization process is thermally activated, the crystallization growth process R is given by:

$$R = R_0 e^{-E_a/k_B T} \dots\dots\dots 1$$

where R₀ is constant. E_a is the overall activation energy, k_B is Boltzmann constant and T is absolute temperature of the samples under laser irradiation. This temperature can be found from Lax formula (9):

$$\Delta T_{max} = \frac{(1-r)N}{(4\pi)^{1/2} \kappa} \left(\frac{P}{\omega}\right) \dots\dots\dots 2$$

where ΔT_{max} is the maximum increase of the surface temperature at the center of the laser spot. r is the reflectivity, κ is the thermal conductivity (W.cm⁻¹K⁻¹), ω is the radius of the laser spot created on the samples, N is a slowly

varying function of the product of absorption coefficient and the laser beam radius, and P is the laser power. The radii of the laser spot, ω , at 4, 6 and 9 W/cm² are calculated to be 0.63, 0.54 and 0.48 cm, respectively.

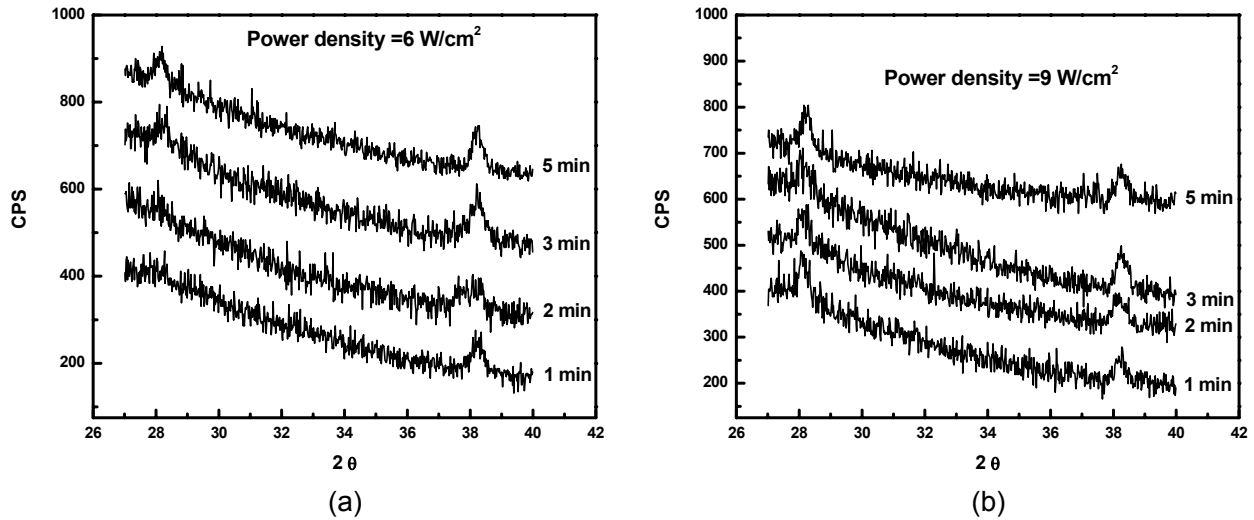


Fig. 4: XRD patterns of the laser annealed samples. Si (111) peak indicates the polycrystalline nature of the films. The laser power density used to irradiate the films at a) 6 W/cm² b) 9 W/cm².

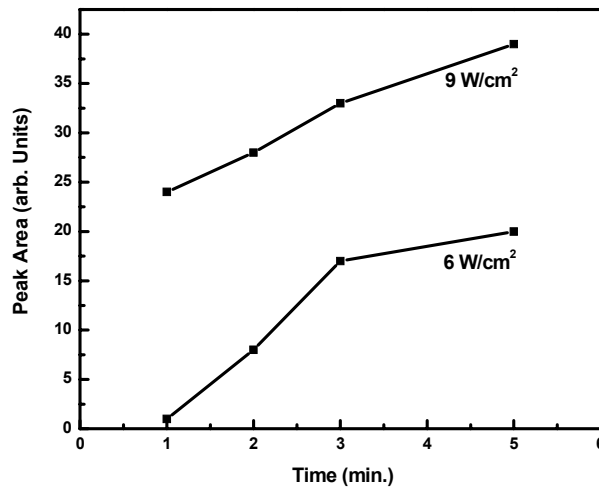


Fig. 5: Peak area vs. annealing laser irradiation time.

According to Lax (9), N in eq. 2 ranges from 0 to 1 depending on the beam radius and the absorption coefficient. For a-Si this factor is than 1 only if the beam sizes less than 5 μm. Since our beam sizes are much larger than this value, N in our samples is taken to be unity.

We turn now to determine a value for the effective thermal conductivity κ of the samples under illumination in eq. 2. It should be mentioned here that in general this value is almost two orders of magnitude lower than that of polycrystalline silicon. Therefore and according to eq. 2, the temperature during illumination is expected to be higher for the amorphous material during laser exposure. This also means that the temperature of the film is expected to decrease during amorphous to crystalline transformation. On the other hand, when the substrate is thick enough, the whole sample (substrate and the deposited films) should be considered when

determining the final heat conductivity in the thin film especially if the film thickness is less than $1.2 \mu\text{m}$ (8). Our films thicknesses are much less than this value, so we will assume that the thermal conductivity changes are not significant enough to affect the temperature rise during laser irradiation. In general, there are four values of thermal conductivity to be considered in the calculations; Al ($2.3 \text{ W/cm}^{-1} \cdot \text{K}^{-1}$), a-Si ($0.01 \text{ W/cm}^{-1} \cdot \text{K}^{-1}$), glass ($0.015 \text{ W/cm}^{-1} \cdot \text{K}^{-1}$) and Kapton ($0.0012 \text{ W/cm}^{-1} \cdot \text{K}^{-1}$). Since the Al thermal conductivity is much higher than the other materials, it will not affect the final effective heat conductivity value. Therefore, the thermal conductivity is estimated to be between that of glass and a-Si in the first set and between Kapton and a-Si in the second set. However, since the thermal conductivity values in the first set are very close to each other, we choose the a-Si value to calculate the temperature increases in these samples. Whereas, in the second set we choose the Kapton thermal conductivity in the calculations since the Kapton substrate thickness is much larger than the amorphous film.

The reflectivity factor in eq. 2 was determined using the silicon and glass indices of refraction at the laser wavelength for the first set and silicon and Kapton indices of refraction in the second set. We obtained 19% reflection at the interface between the glass and silicon. However, with the 4% reflection at the glass air interface side, and neglecting the multiple internal reflections from the glass substrate, the total reflectivity was 18% in the first set. For the second set, we used Kapton FTIR transmission curves to determine its index of refraction. Fig. 6 shows the transmission curve. The obtained index of refraction for the Kapton substrate is 1.8 and hence the total reflectivity in the second set was calculated to be 17%.

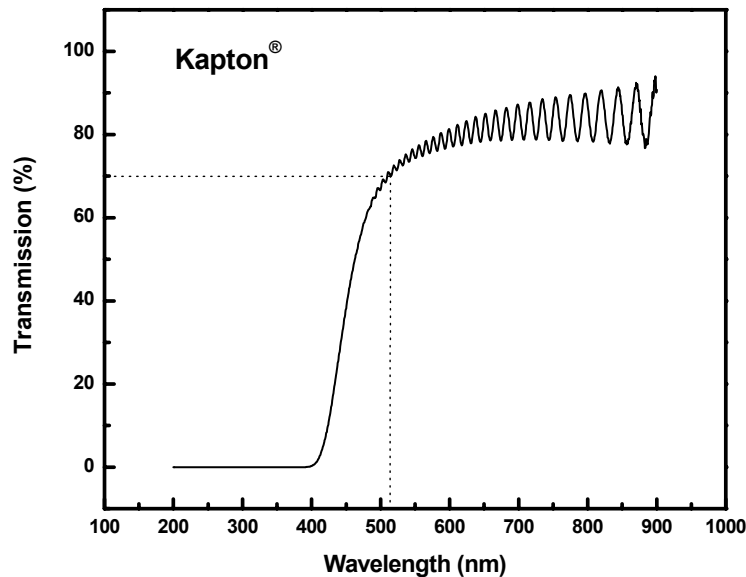


Fig. 6: Transmission curves for the Kapton substrate in the second set. The figure also indicates the transmission at the laser wavelength.

Substituting all these values in eq. 2, the temperature raises during the crystallization process in the first set were 110 , 129 and 144°C at 4 , 6 and 9 W/cm^2 power densities, respectively. Since the calculated values were just corresponding to the temperatures raised by the laser beam on the surface of the sample, the total temperature is obtained by adding the room temperature (25°C) to each value. The temperature rises in the second set were 275 , 414 , and 621°C at 4 , 6 and 9 W/cm^2 power densities, respectively.

Analyzing the results according to the above relations, we obtain a value for the crystallization activation energy of $E_a \approx 0.40 \text{ eV}$. This value is lower than that reported one for Al induced crystallization of a-Si using thermal annealing ($E_a \approx 1.0 \text{ eV}$) [10]. One reason for this low value could be because the laser light has specific

photon energy which is limiting to the crystallization process. However, more research has to be done to investigate the non-thermal effects of lasers in this crystallization process.

Scanning Electron Microscope

Fig. 7 shows the SEM image of the regions in the sample unexposed to the laser beam before and after Al etching. It is clear from this figure that a-Si surface is quite smooth. This is because no interaction occurs when a-Si is in contact with a metal without an excitation source to initiate the crystallization process.

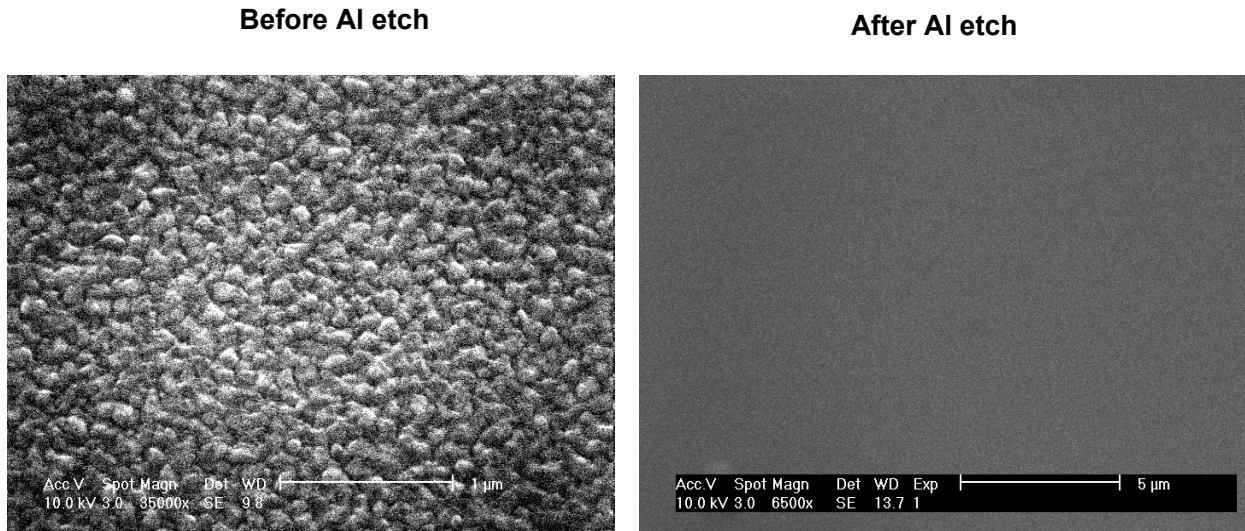


Fig. 7: SEM images of the regions in the samples which were not exposed to the laser beam. The scale in the image after Al etching is higher to show wider regions in the amorphous film.

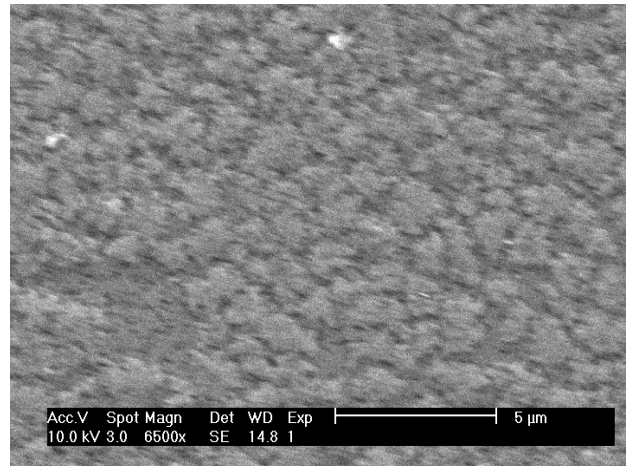
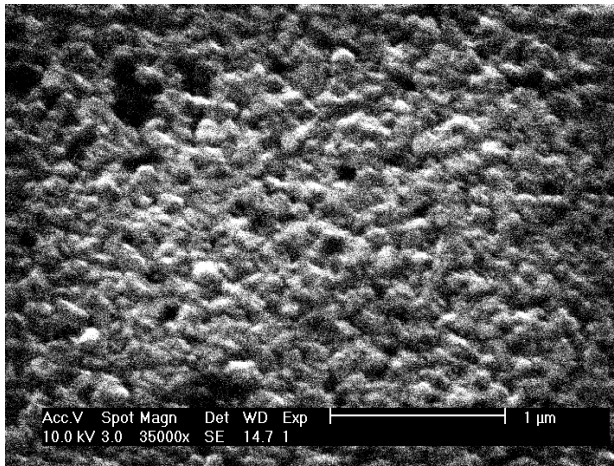
At 4 W/cm^2 , the SEM images were not different than those shown in Fig. 7 for all exposures times, indicating that there was no crystallization at this power density. SEM images of the samples irradiated at 6 and 9 W/cm^2 for 1 , 3 and 5 minutes are shown in Fig. 8 and Fig. 9, respectively. The dendritic growth increases with increase in the laser power density and exposure time as indicated in these figures. The black spots on the Al surface before Al is being etched are mainly composed of silicon as indicated from the EDX pattern shown in Fig. 10.

When the samples are irradiated with the laser beam, the temperature starts to increase rapidly as in the case of conventional thermal annealing. Silicon starts to mix with the Al at the interface between the Si and the Al layers which give raise to a very thin alloy layer of Al and Si. Some of the Si in this layer starts to diffuse through the Al layer and deposit on the top surface. At the same time, Al atoms diffuse through the a-Si thin film and induce the Si atoms in the amorphous matrix to rearrange themselves in more ordered structure in various places. These order structures are the nucleation sites of which silicon grains and dendritic growth initiate. At the same time and separately, some of the silicon in the alloy layer finds its way back to the silicon film and deposits on the surfaces of the newly crystallized regions. The reason for this internal deposition is because crystallized silicon has more stable structure (lower internal energy) than a-Si. Fig. 11 shows an SEM image of the dendritic growth of silicon taken at the edge of laser spot in the amorphous film. The dendritic growth shown in the figure is a result of accumulating silicon that was in the thin alloy layer. When Al is etched off using the etching solution, the alloy layer is also washed off leaving behind poly-Si thin films.

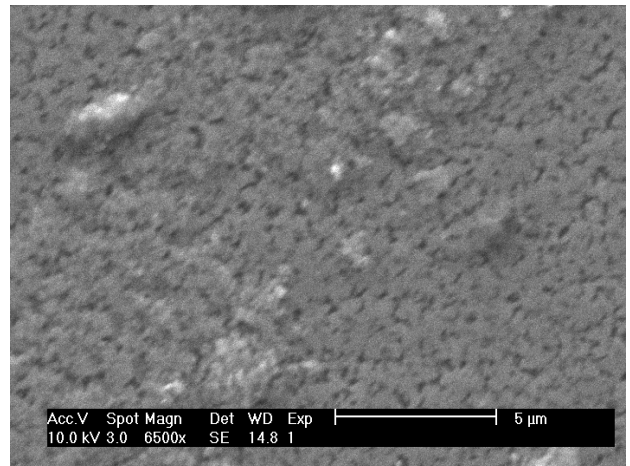
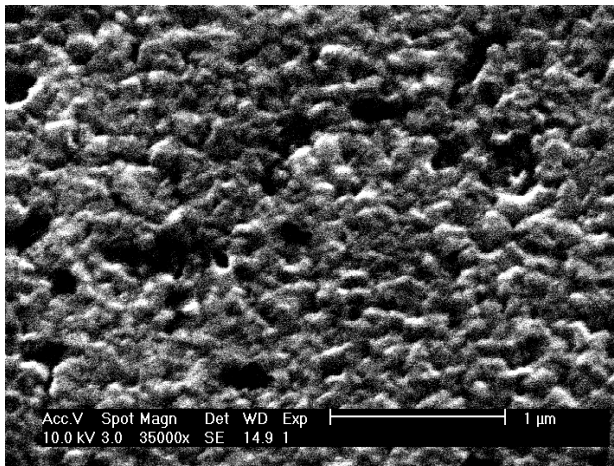
Before Al etch

After Al etch

a



b



c

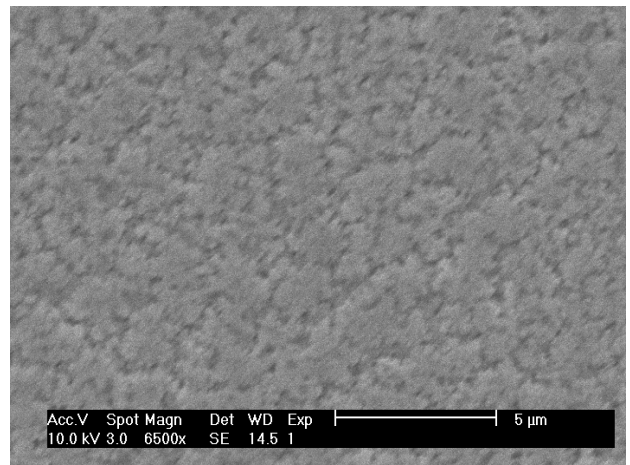
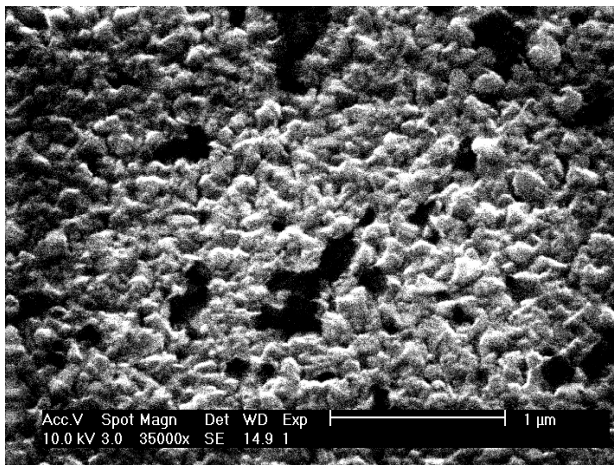
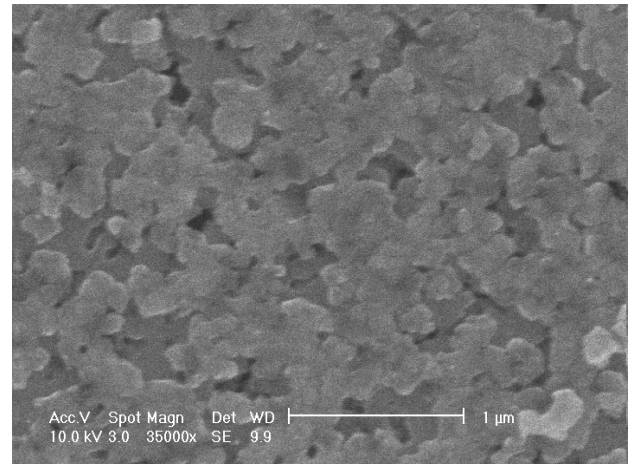
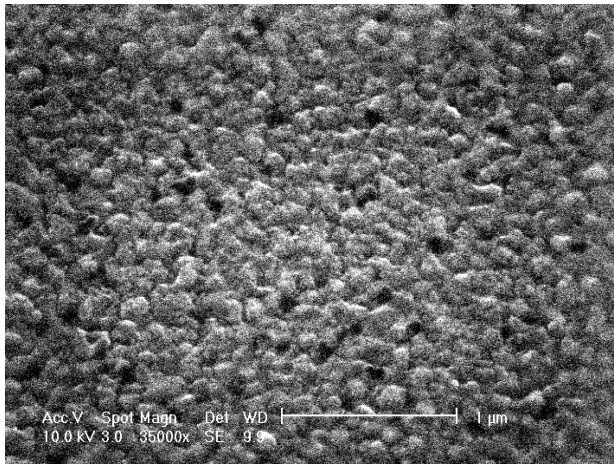


Fig. 8: SEM images of the samples exposed to the 6 W/cm² power density for a) 1 minute b) 3 minutes c) 5 minutes. The scale of the images after Al is etched is higher to show more of the crystallized region.

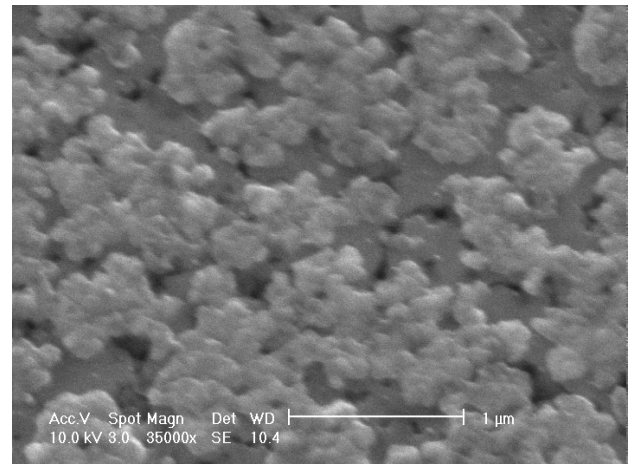
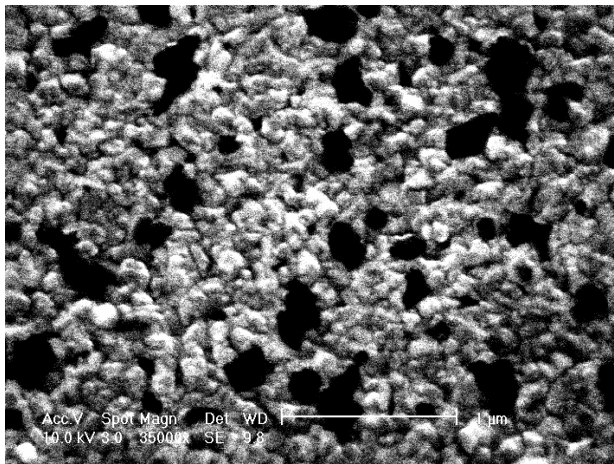
Before Al etch

After Al etch

a



b



c

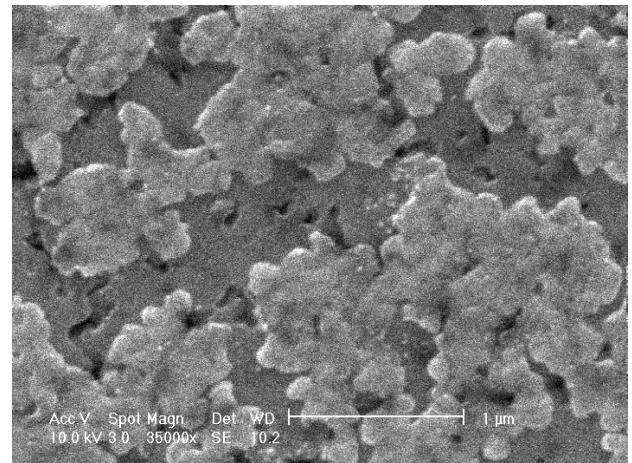
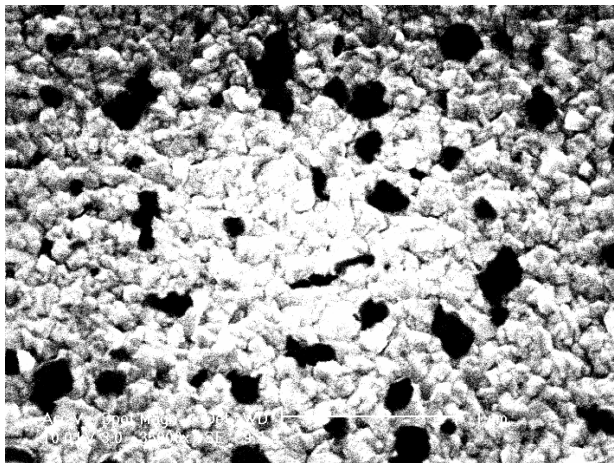


Fig. 9: SEM images of the samples exposed to the 9 W/cm² power density for a) 1 minute b) 3 minutes c) 5 minutes.

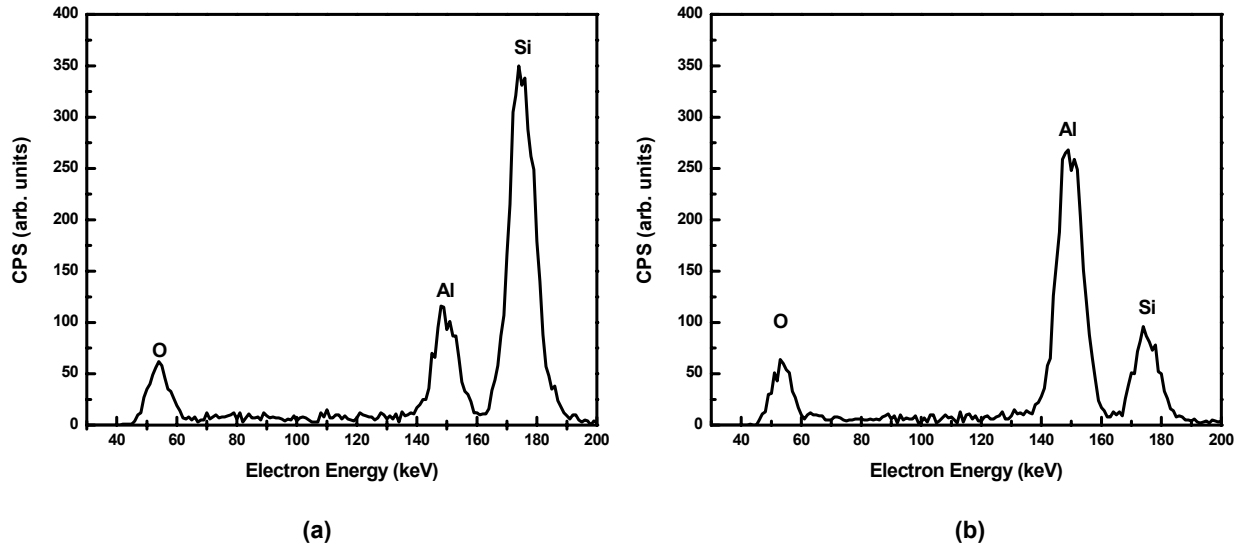


Fig. 10: EDX patterns taken at: a) one of the black spots showing on the Al surfaces in figure 8 and 9, b) on the Al film. The high silicon peak in (a) indicates that this region is mainly composite of silicon that has diffused through the Al layer and deposited on the Al Surface.

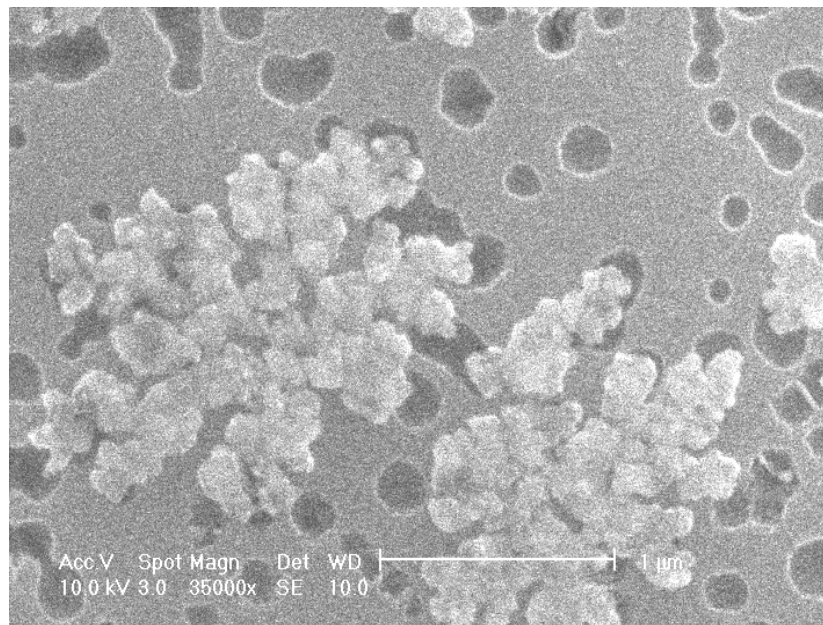


Fig. 11: SEM image of the Si thin film after Al etching. The dark holes in this image are places where silicon has been etched. The dendritic growth shown here is on top of the crystallized regions in the a-Si film.

Fig. 12 shows the SEM images of the Kapton samples. The dendritic growth in the silicon films increase with increasing power density. The images show larger black spots at the Al surface compared to those in the first set. The images also indicate much more violent changes in the surface morphology of these films before Al is etched. This could be explained in terms of the higher temperature increase in the films which lead to fast formation a thick alloy layer.

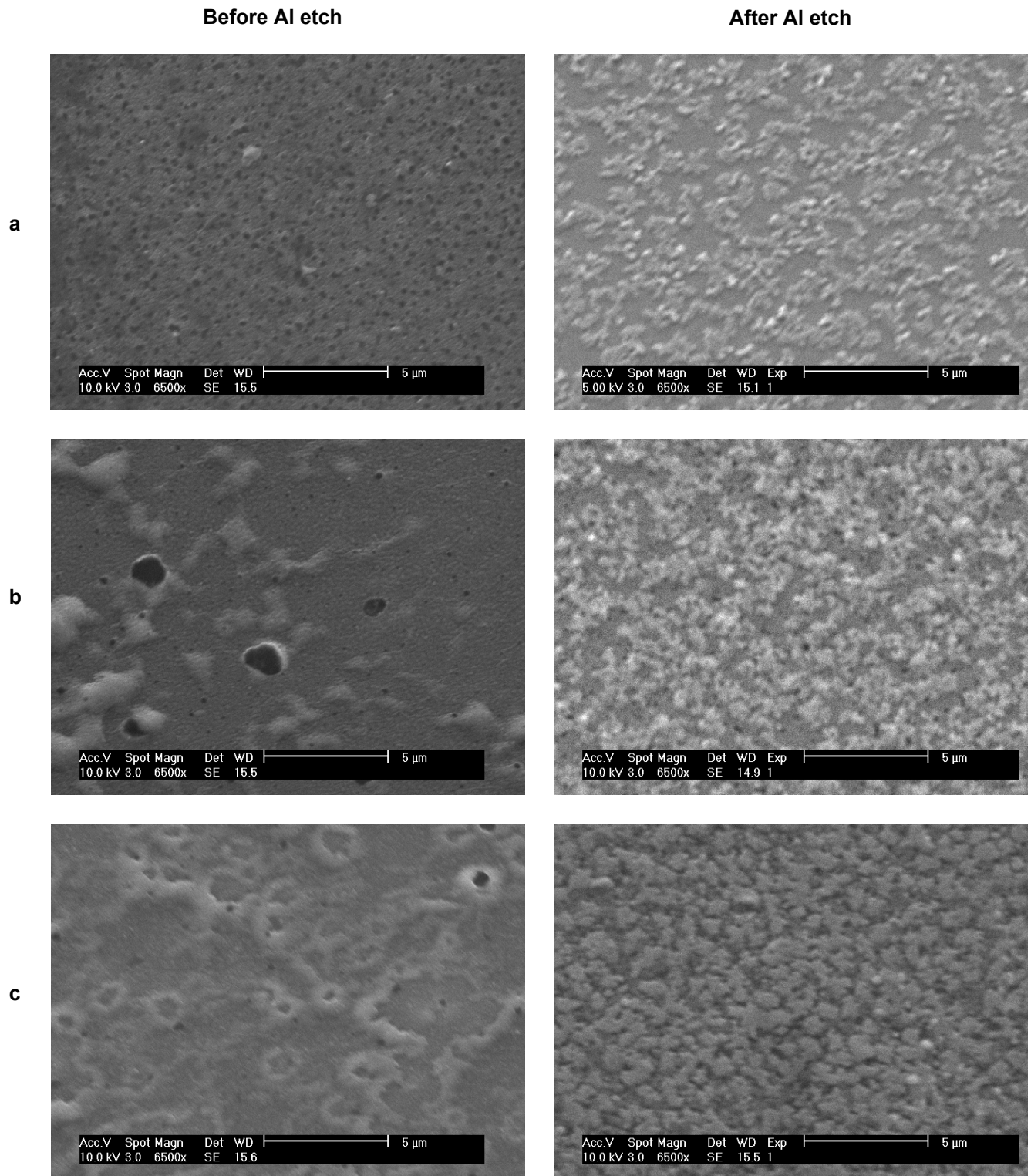


Fig. 12: SEM images of the samples in the second set scanned at laser power density of a) 4 W/cm^2 b) 6 W/cm^2 c) 9 W/cm^2

Schematics of the growth mechanism are shown in Fig. 13. In these schematics, it is showing (Figure 13. (b)) that after prolonged laser exposure time the alloy layer will become very thick, which means that there is enough silicon to fill all the pits that is created during the initial silicon etching process. Also, the dendritic growth will lead eventually to a continuous ploy-Si film as seen in the figure. Nast *et al* also observed the dendritic growth of Si grains in their work (11). Herd *et al* (12) have shown that the dendritic growth behavior of Si grains is common during metal induced crystallization of a-Si at low temperatures.

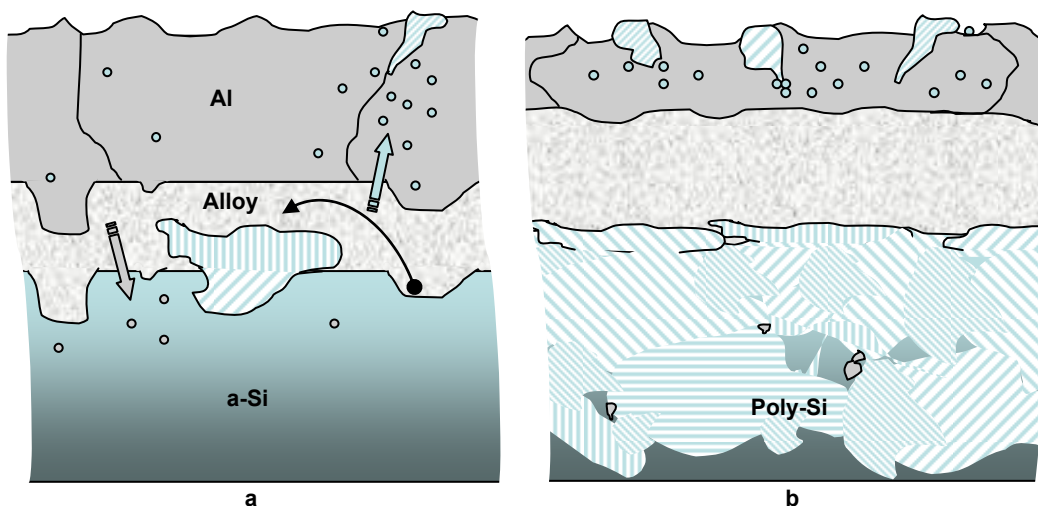


Fig. 13: Schematics of the crystallization mechanism. The small circles indicate the aluminum in the a-Si film and the silicon in the aluminum layer. a) Just after the sample is irradiated with the laser beam, a thin alloy layer of Al and Si is formed at the interface. In this layer silicon deposits on the crystallized regions in the film. b) After prolonged periods of time continuous films are created on the substrate.

Conclusions

Aluminum metal induced crystallization of RF PECVD a-Si:H initiated by Argon-ion laser has been studied. The study revealed that lasers could act as an excitation source in the metal induced crystallization process instead of thermal annealing. The lower activation energy obtained in this process suggests a non-thermal effect in this process, this conclusion needs further investigation. The XRD spectra showed how the crystallized peak area increases both with increasing power density and exposure time. SEM images revealed the changing surface morphology, in the form of increasing dendritic growth, as the samples were exposed to laser beam. The onset power density and exposure time for crystallization were 6 W/cm^2 and 1 minute. Thus, it can be stated that lasers with low power densities can be used as an excitation source in the metal induced crystallization process on flexible substrates.

Acknowledgement

This work has been done with support from the Arkansas Center for Space and Planetary Sciences.

References

1. G. Radnoczi, A. Robertsson, H. T. G. Hentzell, S. F. Gong, and M. A. Hasan, "Al induced crystallization of a-Si", *J. Appl. Phys.* **69**, pp. 6394-6399, 1991
2. A. E. Robertson, L. G. Hultman, H. T. G. Hentzell, S.-E. Hörnström, G. Shaofang, and P. A. Psaras, "Metal induced crystallization of amorphous silicon", *J. Vac. Tech.* **A 5**, pp.1447-1450, 1987
3. S. Lee, Y. Jeon, S. Joo, "Pd induced lateral crystallization of amorphous Si thin films", *Appl. Phys. Lett.* **66**, pp.1671-1673 1671, 1995

4. Soo Y. Yoon, J. Y. Oh, C. O. Kim, J. Jang, "Low temperature solid phase crystallization of amorphous silicon at 380 °C", *J. Appl. Phys.* **84**, pp. 6463-6465, 1998
5. F. A. Quli, J. Singh, "Transmission electron microscopy studies of metal-induced crystallization of amorphous silicon", *Materials Science & Engineering, B: Solid-State Materials for Advanced Technology* **67**, pp.139-144, 1999
6. M. Haque, H. Naseem and W. Brown, "Interaction of aluminum with hydrogenated amorphous silicon at low temperatures", *J. Appl. Phys.* **75**, pp. 3928-3935, 1994
7. T. Y. Choi, D. J. Hwang, C. P. Grioropoulos, "Ultrafast laser-induced crystallization of amorphous silicon films", *Opt. Eng.* **42**, pp. 3383-3388, 2003
8. M. Ivanda, K. Furic, O. Gamulin, M. Persin, and D. Gracin., "cw laser crystallization of amorphous silicon: Thermal or athermal process", *J. Appl. Phys.* **70**, pp. 4637-4639, 1991
9. M. Lax, "Temperature rise induced by a laser beam", *J. Appl. Physics.* **48**, pp. 3919-3924, 1977
10. S. Gall, M. Muske, I. Sieber, O. Nast, W. Fuhs, "Aluminum-induced crystallization of amorphous silicon " *J. Non-crystalline Solids*, **299**, pp. 741-745, 2002
11. O. Nast, S.R. Wenham, "Elucidation of the layer exchange mechanism in the formation of polycrystalline silicon by aluminum-induced crystallization", *J. Appl. Phys.* **88**, pp.124-132, 2000
12. S.R. Herd, P. Chaudhari, M.H. Brodsky, "Metal contact induced crystallization in films of amorphous silicon and germanium", *J. Non- Cryst. Solids* **7**, pp. 309-327, 1972